NATURAL CIRCULATION AND LINEAR STABILITY ANALYSIS FOR LIQUID-METAL REACTORS WITH THE EFFECT OF FLUID AXIAL CONDUCTION

THERMAL HYDRAULICS

KEYWORDS: *linear perturbation analysis, fluid axial heat conduction, liquid metal reactors*

PIYUSH SABHARWALL,[a]* YEON JONG YOO,[b] QIAO WU,[c] and JAMES J. SIENICKI[d]

[a]*Idaho National Laboratory, P.O. Box 1625, Idaho Falls, Idaho 83415-3730*
[b]*NuScale Power, 1100 NE Circle Boulevard, Suite 350, Corvallis, Oregon 97330*
[c]*Oregon State University, Nuclear Engineering Department, Corvallis, Oregon 97330*
[d]*Argonne National Laboratory, 9700 South Cass Avenue, Argonne, Illinois 60439*

Received November 30, 2010
Accepted for Publication August 26, 2011

The effect of fluid axial thermal conduction on one-dimensional liquid metal natural circulation and its linear stability was performed through nondimensional analysis, steady-state assessment, and linear perturbation evaluation. The Nyquist criterion and a root-search method were employed to find the linear stability boundary of both forward and backward circulations. The study provided a relatively complete analysis method for one-dimensional natural circulation problems with the consideration of fluid axial heat conduction. The results suggest that fluid axial heat conduction in a natural circulation loop should be considered only when the modified Peclet number is ~1 or less, which is significantly smaller than the practical value of a lead liquid metal–cooled reactor.

I. INTRODUCTION

Liquid-metal reactors in general can be relatively compact, have a high–power density core, and are economical, thus the modular liquid-metal reactor design. The properties of lead (Pb)/lead-bismuth (Pb-Bi) eutectic (LBE)—mainly its chemical inertness with air and water, high atomic number, low vapor pressure at operating temperatures, and high boiling temperature—offer enhanced safety and reliability compared to sodium-cooled reactors. Forced convection flow is a mature technology, and the low vapor pressure of Pb and Pb-Bi and their inertness offer the possibility to increase the working fluid temperature and plant efficiency while simultaneously reducing plant complexity and cost by employing direct-contact heat transfer systems.[1] This paper provides a relatively complete analysis method for one-dimensional natural circulation problems with the consideration of fluid axial heat conduction.

*E-mail: piyush.sabharwall@inl.gov

Natural convection is of great interest for the development of Generation IV nuclear energy systems because of its vital role in the area of passive safety and reliability. Theoretical and numerical linear stability analysis of single-phase natural convection has been carried out mostly for symmetrically heated and cooled loops.[2–5] These investigations established the theoretical framework of linear stability analysis for natural convection loops.

For an asymmetrically heated/cooled single-phase natural convection loop, which was generally considered to be linearly stable, experimental and numerical studies were also reported.[5–8] It was discovered that instability may occur at a greater temperature change through an asymmetrical heated/cooled natural circulation loop. Conventional light water reactors might not reach such a condition because of the relatively small temperature increase in the core. However, for the development of Generation IV nuclear energy systems, especially for liquid-metal–cooled reactors, significant temperature change in the coolant loop is expected for the purpose of utilizing natural circulation to transport heat at a 100% power rate.

One such system is the Secure Transportable Autonomous Reactor–Liquid Metal (STAR-LM) under development at Argonne National Laboratory. STAR-LM is a 400-MW(thermal) lead-cooled fast reactor that uses lead or LBE coolant and an advanced power conversion system that consists of a gas turbine Brayton cycle utilizing supercritical carbon dioxide to obtain higher plant efficiency. STAR-LM achieves autonomous load following, whereby the core power adjusts itself according to the heat removed without user intervention. This design feature makes it passively safe in that it provides an inherent core shutdown in the event of a loss-of-heat sink accident. More important, the primary coolant loop of this design relies only on natural circulation to eliminate the use of a circulation pump for passive safety consideration. Therefore, it naturally raises the concern of natural circulation instability due to the relatively high temperature change in the reactor core.[9]

To address the instability issue,[10] Wu and Sienicki carried out a one-dimensional linear stability analysis on an LBE natural circulation loop. They found two possible circulation modes, forward and backward. The so-called forward circulation refers to the normal circulation with hot liquid rising through the heated section and falling along the cooling section, whereas the backward circulation flows in the opposite direction, which can be important in the reactor start-up phase. A stable backward circulation is possible if the Reynolds number and the loop friction loss are small. Increasing the minor pressure loss coefficient makes the backward circulation less stable. When a backward circulation reaches its unstable region, since the forward circulation under the same heating/cooling condition is stable, disturbances may grow and result in flow reversal, leading to a stable forward circulation. The results also demonstrated that a forward flow could be linearly unstable if the Reynolds number exceeds a certain critical limit and the minor pressure loss coefficient is small. In reality, flow reversal from the flow instability is unlikely because of the unstable nature of the backward circulation. Under such a circumstance, the nonlinear effects would either calm the disturbance or confine it to a certain magnitude. Moreover, when the forward or backward circulation becomes unstable, the characteristic wavelength is roughly equal to the loop length, almost independent of the circulating speed. This result suggested that an unstable disturbance was enhanced after traveling around the loop, resulting in the growth of its amplitude.

TABLE I

Geometric Parameters of the Natural Circulation Loop

D (m)	H_{core} (m)	H_{HL} (m)	H_{SG} (m)	H_{CL} (m)	L_{HL} (m)	L_{CL} (m)	L (m)
0.063	1.52	3.48	1.52	3.48	4.58	4.58	12.22

However, the effects of the coolant axial heat conduction term were not addressed in the analysis,[10] which raised concerns, since liquid metal is generally referred to as a good thermal conductor. Hence, effort in this study focuses on the analysis of fluid axial thermal conduction for the LBE natural circulation loop of the constant flow area employed in the analysis.[10] The system schematic is shown in Fig. 1a, and the relevant geometric parameters are summarized in Table I (see Nomenclature on p. 316). The investigation will be performed in three

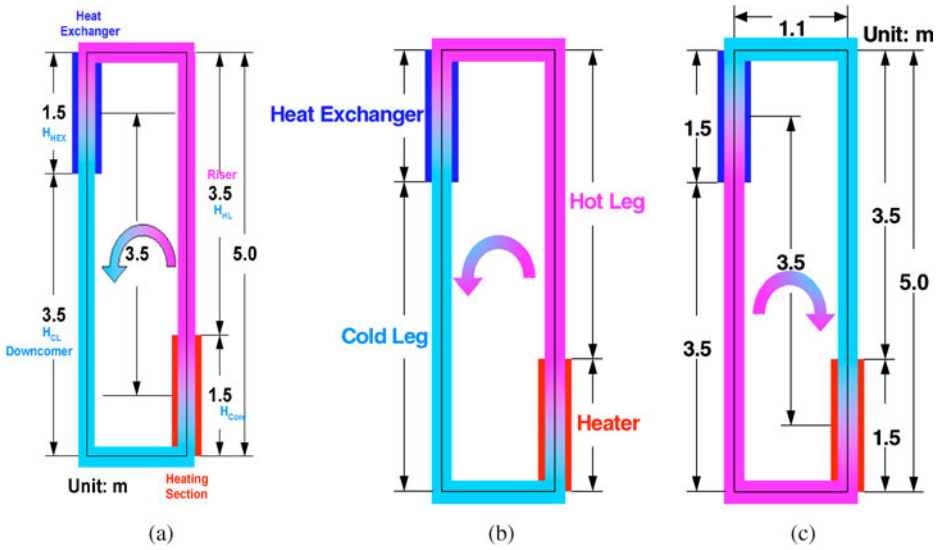

Fig. 1. Schematics of (a) natural convection loop, (b) possible forward circulation direction, and (c) possible backward circulation direction.

steps. First, a dimensionless order-of-magnitude analysis will be presented to address the relative importance of the axial conduction term in the one-dimensional energy equation. Then, the steady-state solution of the natural circulation will be derived to assess the influence of the fluid axial thermal conduction. Finally, a linear perturbation analysis will be performed for a wide range of thermal conductivity coefficients. The analysis is applicable not only for the evaluation of the axial heat conduction effect but also for the development of a solution methodology for natural circulations with a significant axial fluid heat conduction rate.

The so-called forward circulation refers to the normal circulation with hot liquid rising through the heated section and falling along the cooling section, whereas the backward circulation flows in the opposite direction, which can be important in the reactor start-up phase or long-term cooling. As can be seen from the analyses performed,[6] one can infer that instability can happen if the heating power of the two heaters satisfies certain restrictions, eventually resulting in flow reversal. This also was pointed out by previous efforts[5,8] on the stability analysis of asymmetrically heated natural convection loops, which could exist at the reactor start-up phase. This approach is not appropriate for parametric studies on the characteristic frequency and time constant of steady natural convection, also as indicated by a study.[10]

As can be seen from Fig. 1b, under normal conditions, the hot liquid rises through the heater then goes to the hot-leg section followed by a heat exchanger section and then falls into the cold-leg section; Fig. 1c shows the corresponding dimensions of the loop.

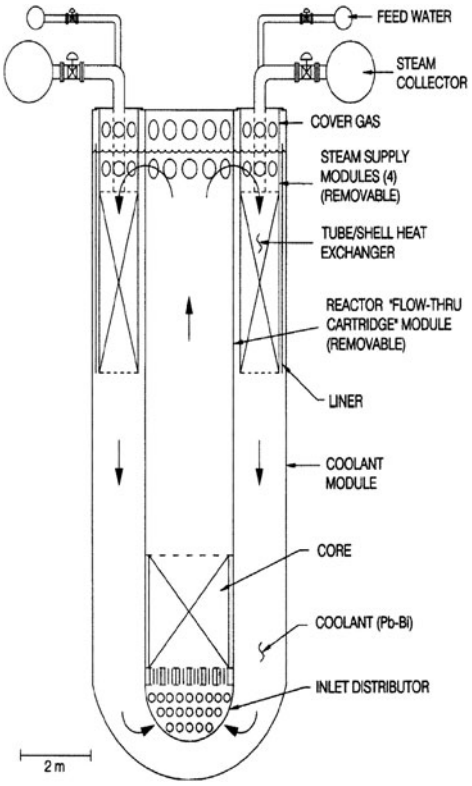

Fig. 2. Schematic of STAR-LM.

II. STAR-LM

In this section, the advanced modular heavy liquid metal coolant (HLMC) reactor concept, STAR-LM, is presented. The STAR project has been proposed by Argonne National Laboratory to meet the need of developing countries for small, multipurpose energy systems.[11,12] The focus of this project was to explore the possibility of addressing proliferation concerns while achieving heightened passive safety and regaining economic competitiveness. The coolant is an HLMC, specifically LBE. The configuration of the STAR-LM concept is illustrated in Fig. 2. There are four key structural elements: the reactor module, the core assembly, the heat exchanger (steam generator) modules, and the coolant module. The reactor core consists of an array of fixed fuel elements. The fuel is uranium nitride with LBE bond fluid. The reference parameters for the 400-MW(thermal) low–power density core include the following: 2.5-m core diameter, 2.0-m active fuel height, 0.5-m fuel element plenum height, 12.7-mm fuel element outside diameter, and 1.47 pitch-to-diameter ratio in triangular lattice. The present study simulates key thermal-hydraulic features of STAR-LM in a vertical natural convection loop using LBE coolant. For simplicity, a one-dimensional model was employed with the assumption of constant pipe size, uniform wall heat flux in the heated section, and constant wall temperature in the heat exchanger section, neglecting the inlet restrictor effect and the form losses due to the bends in the test loop (these losses occur mainly due to bends across the core/heated section and the cold-leg section). The effect of the form losses on the natural convection will be investigated as a future study.

II.A. Lead-Bismuth Eutectic

It is well known that fast reactors show much better neutron economy compared to thermal or epithermal reactors. Low–power density and low–pressure drop core design for the STAR-LM converter introduces the possibility of completely eliminating the main coolant pumps by relying on natural convection for heat transport. The HLMC option has been chosen for STAR-LM because of its attractive inherent safety features (i.e., inertness with air and with the steam/water working fluid) and very high boiling temperature. The LBE (44.5% Pb and 55.5% Bi) alloy can be used as a coolant in the primary circuits of STAR-LM. Table II shows some physical and thermophysical properties characterizing this alloy from the viewpoint of its use as a coolant.

TABLE II

Physical and Thermophysical Properties of LBE and Dependence of Some Properties on Temperature*

Parameter	Temperature (K)					
	403	473	573	673	773	873
Density (kg/m^3)	10 570	10 486	10 364	10 242	10 120	10 000
Heat capacity (J/kg·K)	146	146	146	146	146	146
Kinematic viscosity ($\times 10^8$) (m^3/s)	31.4	24.3	18.7	15.7	13.6	12.4
Prandtl number ($\times 10^2$) (Pr)	4.45	3.18	2.24	1.72	1.37	1.15
Heat conductivity (W/m·K)	10.93	11.74	12.67	13.72	14.65	15.81
Thermal diffusivity ($\times 10^6$) (m^2/s)	7.1	7.6	8.3	9.1	9.9	10.8
Melting temperature (K)	398					
Boiling temperature (K)	1943					

*From Ref. 13.

Compared to other liquid metals used for the same purposes, its high density and the high boiling temperature are noteworthy. The latter property is the obvious advantage of this coolant, because it enhances the reliability and safety of the reactor. It is worth noting that the chemical activity of the coolant to water, steam, and air (i.e., to substances that can interact with the coolant in some accident conditions) is relatively low. However, it has long been considered that LBE may not be suitable as a reactor coolant because of corrosion problems. The corrosion problem can be solved by choosing the proper material, temperature, fluid velocity, and oxygen concentration. The use of ferritic stainless steel in the core and hot-leg regions with oxide layer corrosion protection is regarded as a proven technology, and austenitic stainless steel can be adopted in the cold-leg regions, including the vessel.

II.B. Comparison of LBE, Lead, and Sodium

The common objectives of sodium-cooled and lead-cooled fast reactors are to achieve better economics than with alternative systems, to find an optimal solution for the back-end fuel cycle, and to achieve a high degree of safety and reliability (see Table III). Lead-bismuth and Pb are chemically passive, so neither fire nor explosion is possible in case they interact with water. The Na-H_2O reaction is violent and calls for installing an intermediate heat transport system (IHTS) between primary and secondary circuits. In the case of Pb- or Pb-Bi-cooled reactor systems, an IHTS is not necessary, which suggests that a steam generator could be placed in direct contact with the primary circuit coolant.

II.C. The Argonne Lead Loop Facility

The Argonne Lead Loop Facility (ALLF) simulates key thermal-hydraulic features of STAR-LM in a vertical natural convection loop using LBE coolant and stainless steel structure. The LBE inside the test loop will be heated by seven fuel rod simulators having a 36-in.-high heated zone. Heat will be rejected from the LBE in the loop to a heat exchanger in which subcooled water is the heat sink. The water will flow through a 0.625-in.-diam copper cooling coil bent into a helical spiral surrounding the pipe wall. The reference thermal-hydraulic conditions for ALLF are shown in Table IV.

TABLE III

Thermophysical Properties of Sodium, Lead, and Lead-Bismuth*

Property	Na	Pb	Pb-Bi (Eutectic)
Melting temperature (°C)	98	327.4	125
Boiling temperature (°C)	883	1 745	1 670
Heat of melting (kJ/kg)	114.8	24.7	38.8
Heat of vaporization (kJ/kg)	3871	856.8	852
Density (kg/m^3)	845	10 520	10 150
Heat capacity (kJ/kg·°C)	1.269	0.147	0.146
Kinematic viscosity (m^2/s)	3×10^7	1.9×10^7	1.4×10^7
Surface tension (mN/m)	163	480	392

*From Ref. 14.

III. MATHEMATICAL MODEL

Figure 3 is a schematic diagram of the ALLF to be investigated. It contains primarily four parts: the heated section, the upper pool, the cooling section, and an inlet restriction unit.

For simplicity, a one-dimensional analysis is performed, neglecting heat losses and taking axial heat conduction of the fluid into consideration. Fluid properties are considered constant except for the effect of density variations in producing buoyancy. For this purpose,

TABLE IV

Comparison of Reference Thermal-Hydraulic Conditions for STAR-LM with ALLF

	STAR-LM	ALLF
Power (MW)	400	0.206
Temperature rise across heated zone (°C)	183	85
Coolant inlet temperature (°C)	291	269.4
Coolant outlet temperature (°C)	474	354.4
Coolant velocity through rod array (m/s)	0.383	0.501

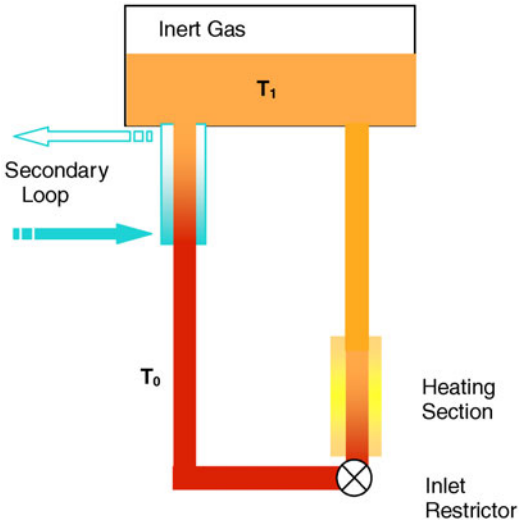

Fig. 3. Schematic diagram of the circulation loop.

density is related to temperature according to the Boussinesq state approximation:

$$\rho = \rho_0[1 - \beta(T - T_0)] \ , \tag{1}$$

where ρ_0 is a nominal value of the density corresponding to a reference temperature T_0. The governing equations are given by

continuity equation:

$$\frac{\partial \rho}{\partial t} + \frac{\partial(\rho u)}{\partial s} = 0 \tag{2}$$

momentum balance equation:

$$\rho\left(\frac{\partial u}{\partial t} + u\frac{\partial u}{\partial s}\right) = -\frac{\partial \rho}{\partial s} + \rho g_s - \tau_w\left(\frac{P}{A}\right) \tag{3}$$

energy balance equation:

$$\rho C\frac{DT}{Dt} - k\frac{\partial^2 T}{\partial s^2} = \begin{cases} q_w''(P_h/A) & \text{Heating} \\ -\dfrac{h(T - T_w)P_h}{A} & \text{Cooling} \\ 0 & \text{Adiabatic} \end{cases} . \tag{4}$$

The relevant constitutive relations are

wall friction:

$$\tau_w = f\tfrac{1}{2}\rho_0 u^2 \tag{5}$$

wall heat transfer:

$$\text{Nu} = 0.625(\text{Re}\,\text{Pr})^{0.4} \tag{6}$$

friction factor:

$$f = \frac{a}{\text{Re}^n} \ .$$

The nondimensional groups are defined as

Nusselt number:

$$\text{Nu} = \frac{hD}{k}$$

Reynolds number:

$$\text{Re} = \frac{\rho u D}{\mu}$$

Prandtl number:

$$\text{Pr} = \frac{\mu C}{k} \ .$$

Because of the high fluid density, the flow to be dealt with is mostly in a turbulent regime with $a = 0.317$ and $n = 0.25$, whereas for laminar flows $a = 16$ and $n = 1$. The subscript zero refers to a reference condition, usually taken at the inlet of the heated section. The heating and cooling occur at the pipe wall, whereas the unheated sections are considered to be adiabatic. A constant heat exchanger wall temperature is assumed because of the boiling heat transfer in the secondary loop at a near-atmospheric condition. The fluid properties are treated as constants at the mean coolant temperature, except for the fluid density that is subject to the Boussinesq state approximation.

III.A. Dimensionless Analysis

The effect of the axial thermal heat conductivity is determined by the heat conduction term in the energy balance equation. Its nondimensional form is given by

$$\frac{DT^+}{Dt^+} - \left(\frac{k}{\rho_0 C u_i L_i}\right)\frac{\partial^2 T^+}{\partial s^{+2}} = \begin{cases} \left(\dfrac{q_w'' P_h L_i}{\rho_0 C u_i A (T_H - T_C)}\right) \\ -(T^+ - T_W^+)\left(\dfrac{h P_h L_i}{\rho_0 C u_i A}\right) \\ 0 \ . \end{cases} \tag{7}$$

The nondimensional parameters are defined as

$$T^+ = T/(T_H - T_C) \ ,$$

$$s^+ = s/L_i \ ,$$

and

$$t^+ = t/(L_i/u_i) \ ,$$

where L_i, u_i, and $(T_H - T_C)$ are the reference parameters, representing the section length, fluid velocity, and maximum temperature difference in the loop, respectively. To address the effect of the axial heat conduction term, its order of magnitude ought to be compared with the term of energy transport due to fluid flow, which is represented by a modified Peclet number of each section, defined as

$$\mathrm{Pe}_i = \left(\frac{\rho_0 C u_i L_i}{k}\right) = \mathrm{Re}_{D,i}\mathrm{Pr}\left(\frac{L}{D}\right)_i \ . \tag{8}$$

When the Peclet number is very large, the energy transport rate through fluid flow is greater than the axial heat conduction rate, and thus the axial conduction term becomes less important. For natural circulation at low-power conditions, the fluid velocity is small, and the axial conduction term becomes more important. Such a situation may be particularly important for reactor early start-up or shutdown with decay power.

In Fig. 4, the Peclet number of the heated/cooled region of the test loop is presented as a function of the Reynolds number. For the thermal conductivity of LBE in the specified circulation loop, only when Re drops below 3×10^3 does the core Peclet number become <1. Generally speaking, one expects to consider the axial heat conduction term when the Peclet number is ~ 1 or less, which is significantly smaller than the practical value (100 000 in the specified loop) of liquid metal natural circulation systems. Therefore, it is appropriate to neglect the fluid axial heat conduction effect in the thermal-hydraulic analysis related to liquid metal natural circulation–cooled nuclear reactors. However, at low heating power conditions (at decay heat power level $\sim$3% of nominal power), as in the case of reactor start-up after shutdown, fluid axial thermal conduction could become important because of the slow coolant natural circulation. In those cases, the magnitude of the system Peclet number should be closely examined to validate neglecting the fluid axial heat conduction in natural circulation analysis.

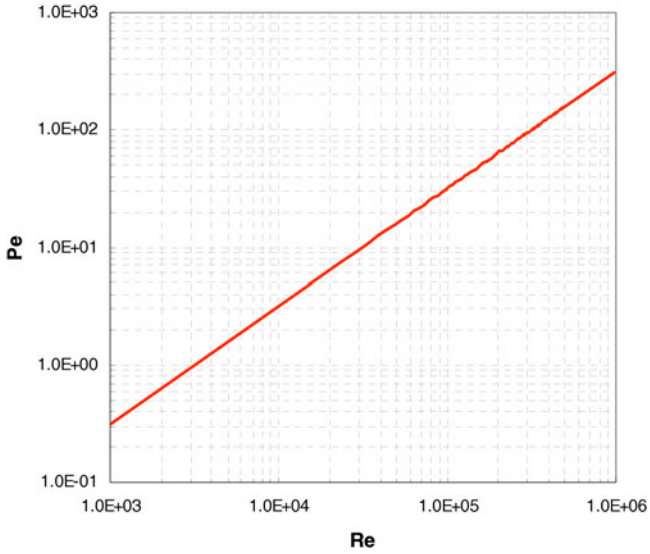

Fig. 4. Peclet number versus Reynolds number.

III.B. Steady-State Analysis

For steady-state conditions, Eq. (2) suggests that the mass flux ρu is constant in each pipe section. Using the mass flux in the heated region as the representative parameter, we have the mass flux in any pipe section (section i):

$$(\rho u)_{core,s} = (\rho u)_{i,s}\left(\frac{A_{core}}{A_i}\right) \ . \tag{9}$$

Integrating Eq. (3) around the loop under steady-state conditions gives

$$\oint \rho g_s \, ds - \oint \tau_w \left(\frac{P}{A}\right) ds = 0 \ , \tag{10}$$

which indicates that the friction force is balanced by buoyancy force. The wall shear stress is given by

$$\tau_w = f\tfrac{1}{2}\rho_0 u_s^2 \ , \tag{11}$$

where the friction factor f is generally correlated by

$$f = \frac{a}{\mathrm{Re}^n} = \left[\frac{a\mu^n}{(\rho_0 D)^n}\right] u_s^{-n} \ . \tag{12}$$

Therefore, Eq. (10) can be further reduced to

$$-\rho_0 \beta g \oint T_s (g_s/g)\, ds - \frac{1}{2}\rho_0 u_{core,s}^2 \times \sum_i \left\{ \left(\frac{A_{core}}{A_i} \right)^2 \left[a \left(\frac{\mu}{\rho_0 D u_s} \right)^n \left(\frac{PS}{A} \right) + k \right]_i \right\} = 0 \ , \tag{13}$$

with k_i representing the minor pressure loss at the end of each pipe section. The equation needs the solution of temperature distribution around the loop.

Under steady-state conditions, Eq. (4) can be integrated in each pipe section:

Heated section:

$$\rho C \left[\frac{\partial T}{\partial t} + u \frac{\partial T}{\partial s} \right] = q_w'' \left(\frac{P_h}{A} \right) + k \frac{d^2 T}{ds^2} \ ,$$

$$0 \le s \le H_{core} \ , \tag{14}$$

$$T = N_2 s + B_1 e^{-N_1 (H_{core} - s)} + B_2 \ , \tag{15}$$

$$\frac{dT}{ds} = N_2 + N_1 B_1 e^{-N_1 (H_{core} - s)} \ , \tag{16}$$

$$N_1 = \left(\frac{\rho c u}{k} \right)_{core} \ ,$$

$$N_2 = \left(\frac{q_w''}{\rho c u} \right)_{core} \left(\frac{P_h}{A} \right)_{core} \ .$$

Hot section:

$$\frac{d^2 T}{ds^2} - \frac{\rho C u}{k} \frac{dT}{ds} = 0 \ , \quad 0 \le s \le L_{HL} \ , \tag{17}$$

$$T = B_3 e^{-N_1 (L_{HL} - s)} + B_4 \ , \tag{18}$$

$$\frac{dT}{ds} = B_3 N_1 e^{-N_1 (L_{HL} - s)} \ . \tag{19}$$

Heat exchanger section:

$$\rho C u \frac{dT}{ds} = -(T - T_w) h \left(\frac{P_h}{A} \right) + k \frac{d^2 T}{ds^2} \ ,$$

$$0 \le s \le H_{SG} \ , \tag{20}$$

$$T = B_5 e^{N_1 \Lambda_1 s} + B_6 e^{-N_1 \Lambda_2 (H_{SG} - s)} + T_w \ , \tag{21}$$

$$\frac{dT}{ds} = (N_1 \Lambda_1) B_5 e^{N_1 \Lambda_1 s} + N_1 \Lambda_2 B_6 e^{-N_1 \Lambda_2 (H_{SG} - s)} \ , \tag{22}$$

$$\Lambda_1 = \frac{1}{2} - \sqrt{\left(\frac{1}{4} \right) + \left(\frac{h (P_h/A)_{SG} k}{(\rho c u)^2} \right)} \ ,$$

$$\Lambda_2 = \frac{1}{2} + \sqrt{\left(\frac{1}{4} \right) + \left(\frac{h (P_h/A)_{SG} k}{(\rho c u)^2} \right)} \ .$$

Cold section:

$$\frac{d^2 T}{ds^2} - \frac{\rho C u}{k} \frac{dT}{ds} = 0 \ , \quad 0 \le s \le L_{CL} \ , \tag{23}$$

$$T = B_7 e^{-N_1 (L_{CL} - s)} + B_8 \ , \tag{24}$$

$$\frac{dT}{ds} = N_1 B_7 e^{-N_1 (L_{CL} - s)} \ . \tag{25}$$

The coefficients B_1 through B_8 can be determined by imposing temperature and flux continuity as the boundary condition at each pipe junction:

$$T\big|_{s=L_{CL}}^{CL} = T\big|_{s=0}^{core} \ ,$$

$$T\big|_{s=H_{core}}^{core} = T\big|_{s=0}^{HL} \ ,$$

$$T\big|_{s=L_{HL}}^{HL} = T\big|_{s=0}^{SG} \ ,$$

$$T\big|_{s=H_{SG}}^{SG} = T\big|_{s=0}^{CL} \ ,$$

$$\left. \frac{dT}{ds} \right|_{s=L_{CL}}^{CL} = \left. \frac{dT}{ds} \right|_{s=0}^{core} \ ,$$

$$\left. \frac{dT}{ds} \right|_{s=H_{core}}^{core} = \left. \frac{dT}{ds} \right|_{s=0}^{HL} \ ,$$

$$\left. \frac{dT}{ds} \right|_{s=L_{HL}}^{HL} = \left. \frac{dT}{ds} \right|_{s=0}^{SG} \ ,$$

and

$$\left. \frac{dT}{ds} \right|_{s=H_{SG}}^{SG} = \left. \frac{dT}{ds} \right|_{s=0}^{CL} \ .$$

However, depending on the flow direction, the integration is different, and therefore two separate cases should be investigated depending on the flow directions, i.e.,

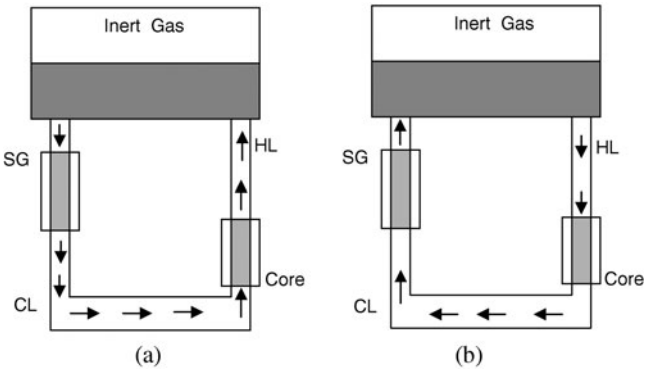

Fig. 5. (a) Forward and (b) backward circulation flow loops.

forward and backward circulations, as illustrated in Fig. 5. The so-called forward circulation, shown in Fig. 5a, refers to the normal circulation with hot liquid rising above the heated section and falling along the cooling section, whereas the backward circulation, shown in Fig. 5b, flows in the opposite direction.

III.B.1. Forward Circulation

For forward circulation, substituting the eight boundary conditions into the solutions of temperature distribution, we have the following equations that govern the eight constants:

$$B_1 + B_2 - B_3 e^{-N_1 L_{HL}} - B_4 = -N_2 H_{core} \ , \tag{26}$$

$$-B_3 N_1 e^{-N_1 L_{HL}} + N_1 B_1 = -N_2 \ , \tag{27}$$

$$B_3 + B_4 - B_5 - B_6 e^{-N_1 \Lambda_2 H_{SG}} = T_w \ , \tag{28}$$

$$B_3 N_1 - B_5 N_1 \Lambda_1 - B_6 N_1 \Lambda_2 e^{-N_1 \Lambda_2 H_{SG}} = 0 \ , \tag{29}$$

$$B_5 e^{N_1 \Lambda_1 H_{SG}} + B_6 - B_7 e^{-N_1 L_{CL}} - B_8 = -T_w \ , \tag{30}$$

$$(N_1 \Lambda_1) B_5 e^{N_1 \Lambda_1 H_{SG}} + (N_1 \Lambda_2) B_6 - N_1 B_7 e^{-N_1 L_{CL}} = 0 \ , \tag{31}$$

$$B_7 + B_8 - B_1 e^{-N_1 H_{core}} - B_2 = 0 \ , \tag{32}$$

$$B_7 N_1 - B_1 N_1 e^{-N_1 H_{core}} = N_2 \ , \tag{33}$$

and

$$\begin{bmatrix} 1 & 1 & -e^{-N_1 L_{HL}} & -1 & 0 & 0 & 0 & 0 \\ N_1 & 0 & -N_1 e^{-N_1 L_{HL}} & 0 & 0 & 0 & 0 & 0 \\ 0 & 0 & 1 & 1 & -1 & -e^{-N_1 \Lambda_2 H_{SG}} & 0 & 0 \\ 0 & 0 & N_1 & 0 & -N_1 \Lambda_1 & -N_1 \Lambda_2 e^{-N_1 \Lambda_2 H_{SG}} & 0 & 0 \\ 0 & 0 & 0 & 0 & e^{N_1 \Lambda_1 H_{SG}} & 1 & -e^{-N_1 L_{CL}} & -1 \\ 0 & 0 & 0 & 0 & N_1 \Lambda_1 e^{N_1 \Lambda_1 H_{SG}} & N_1 \Lambda_2 & -N_1 e^{-N_1 L_{CL}} & 0 \\ -e^{-N_1 H_{core}} & -1 & 0 & 0 & 0 & 0 & 1 & 1 \\ -N_1 e^{-N_1 H_{core}} & 0 & 0 & 0 & 0 & 0 & N_1 & 0 \end{bmatrix} \begin{bmatrix} B_1 \\ B_2 \\ B_3 \\ B_4 \\ B_5 \\ B_6 \\ B_7 \\ B_8 \end{bmatrix}$$

$$= \begin{bmatrix} -N_2 H_{core} \\ -N_2 \\ T_w \\ 0 \\ -T_w \\ 0 \\ 0 \\ N_2 \end{bmatrix} \ , \tag{34}$$

where

$$N_1 = \left(\frac{\rho cu}{k}\right)_{core} ,$$

$$B_5 = C_6 e^{N_1 \Lambda_1 H_{SG}} ,$$

$$\Lambda_1 = \frac{1}{2} - \sqrt{\left(\frac{1}{4}\right) + \left(\frac{h(P_h/A)_{SG}\, k}{(\rho cu)^2}\right)} ,$$

$$N_2 = \left(\frac{q''_w}{\rho cu}\right)_{core} \left(\frac{P_h}{A}\right)_{core} ,$$

$$B_6 = C_7 e^{N_1 \Lambda_2 H_{SG}} ,$$

$$\Lambda_2 = \frac{1}{2} + \sqrt{\left(\frac{1}{4}\right) + \left(\frac{h(P_h/A)_{SG}\, k}{(\rho cu)^2}\right)} ,$$

$$B_1 = C_1 e^{N_1 H_{core}} ,$$

$$B_7 = C_9 e^{N_1 L_{CL}} ,$$

$$B_2 = C_2 ,$$

$$B_8 = C_{10} ,$$

and

$$B_3 = C_4 e^{N_1 L_{HL}}$$

Now from the buoyancy term equation (momentum equation) for the forward circulation loop, we have

$$\begin{aligned}
-\oint T g_s \rho_0 \beta \, ds &= -\left[\rho_0 \beta \left(\int_0^{H_{core}} T_{core} + \int_0^{H_{HL}} T_{HL} + \int_0^{H_{SG}} T_{SG} + \int_0^{H_{CL}} T_{CL} \right)\right] \\
&= \left[-\rho_0 \beta \left(\int_0^{H_{core}} T_{core}(-1) + \int_0^{H_{HL}} T_{HL}(-1) + \int_0^{H_{SG}} T_{SG}(1) + \int_0^{H_{CL}} T_{CL}(1) \right)\right] \\
&= \left[\rho_0 \beta \left(\int_0^{H_{core}} T_{core} + \int_0^{H_{HL}} T_{HL} - \int_0^{H_{SG}} T_{SG} - \int_0^{H_{CL}} T_{CL} \right)\right] \\
&= \left[\rho_0 \beta \left(\frac{N_2 H_{core}^2}{2} + \frac{B_1}{N_1} + B_2 H_{core} - \frac{B_1 e^{-N_1 H_{core}}}{N_1} + \frac{B_3 e^{-N_1 (L_{HL} - H_{HL})}}{N_1} + B_4 H_{HL} \right.\right. \\
&\quad - \frac{B_3 e^{-N_1 L_{HL}}}{N_1} - \frac{B_5 e^{N_1 \Lambda_1 H_{SG}}}{N_1 \Lambda_1} - \frac{B_6}{N_1 \Lambda_2} - T_w H_{SG} + \frac{B_5}{N_1 \Lambda_1} + \frac{B_6 e^{-N_1 \Lambda_2 H_{SG}}}{N_1 \Lambda_2} \\
&\quad \left.\left. - \frac{B_7 e^{-N_1 (L_{CL} - H_{CL})}}{N_1} - B_8 H_{CL} + \frac{B_7 e^{-N_1 L_{CL}}}{N_1} \right)\right] . \qquad (34)
\end{aligned}$$

By substituting this closed-loop temperature integration into the integral momentum equation, an algebraic equation of the fluid velocity is obtained.

III.B.2. Backward Circulation

For backward circulation, the buoyancy term in the integral momentum equation is different from that obtained in the case of forward circulation:

$$\begin{aligned}
-\oint T g_s \rho_0 \beta \, ds &= -\left[\rho_0 \beta \left(\int_0^{H_{core}} T_{core} + \int_{L_{CL} - H_{CL}}^{L_{CL}} T_{HL} + \int_0^{H_{SG}} T_{SG} + \int_{L_{HL} - H_{HL}}^{L_{HL}} T_{CL} \right)\right] \\
&= \left[-\rho_0 \beta \left(\int_0^{H_{core}} T_{core}(1) + \int_{L_{CL} - H_{CL}}^{L_{CL}} T_{HL}(-1) + \int_0^{H_{SG}} T_{SG}(-1) + \int_{L_{HL} - H_{HL}}^{L_{HL}} T_{CL}(1) \right)\right] \\
&= \left[\rho_0 \beta \left(- \int_0^{H_{core}} T_{core} + \int_{L_{CL} - H_{CL}}^{L_{CL}} T_{HL} + \int_0^{H_{SG}} T_{SG} - \int_{L_{HL} - H_{HL}}^{L_{HL}} T_{CL} \right)\right]
\end{aligned}$$

$$= \left[\rho_0 \beta \left(\frac{-N_2 H_{core}^2}{2} - \frac{B_1}{N_1} - B_2 H_{core} + \frac{B_1 e^{-N_1 H_{core}}}{N_1} + \frac{B_3 e^{-N_1 (L_{HL} - L_{CL})}}{N_1} - \frac{B_3 e^{-N_1 (L_{HL} - L_{CL} + H_{CL})}}{N_1} \right.\right.$$
$$+ B_4 H_{CL} + \frac{B_5 e^{N_1 \Lambda_1 H_{SG}}}{N_1 \Lambda_1} + \frac{B_6}{N_1 \Lambda_2} + T_w H_{SG} - \frac{B_5}{N_1 \Lambda_1} - \frac{B_6 e^{-N_1 \Lambda_2 H_{SG}}}{N_1 \Lambda_2} - \frac{B_7 e^{-N_1 (L_{CL} - L_{HL})}}{N_1}$$
$$\left.\left. - B_8 L_{HL} + \frac{B_7 e^{-N_1 (L_{CL} - L_{HL} + H_{HL})}}{N_1} + B_8 (L_{HL} - H_{HL}) \right) \right] . \quad (35)$$

For both forward and backward circulation we have for the friction term

$$f_2 \left(\frac{L}{D} \right) \rho_0 u^2 . \quad (36)$$

If $\mathrm{Re} < 2100$,

$$f = \left(\frac{64}{4} \right) \mathrm{Re}^{-1} , \quad (37)$$

which is the Fanning friction factor for the laminar flow.

If $(\mathrm{Re} \geq 2100)$ and $(\mathrm{Re} < 30\,000)$,

$$f = \frac{0.316}{4} (\mathrm{Re})^{-0.25} , \quad (38)$$

which is the Fanning friction factor for the turbulent flow.

If $\mathrm{Re} > 30\,000$,

$$f = \left(\frac{0.184}{4} \right) (\mathrm{Re})^{-0.20} , \quad (39)$$

which is the Fanning friction factor for the turbulent flow.

Using the new fluid temperature as the input, iteration continues until the solution converges:

$$\frac{\oint (T g_s \rho_0 \beta)_{FC} \, ds - \frac{f}{2} \left(\frac{L}{D} \right) \rho_0 u^2}{\frac{f}{2} \left(\frac{L}{D} \right) \rho_0 u^2} = \in \quad (40)$$

and

$$\frac{\oint (T g_s \rho_0 \beta)_{BC} \, ds - \frac{f}{2} \left(\frac{L}{D} \right) \rho_0 u^2}{\frac{f}{2} \left(\frac{L}{D} \right) \rho_0 u^2} = \in , \quad (41)$$

where FC and BC refer to the forward circulation and backward circulation for the loop, respectively. The value of u is iterated such that $\in < 0.00001$ condition is satisfied and thus steady-state velocity and steady-state temperature are obtained and further used in the perturbation analysis.

III.B.3. Steady-State Solutions

In Fig. 6, the temperature profiles of forward and backward natural circulations are presented, with a nominal power of 0.206 MW. As the modified Peclet number decreases (corresponding to an artificial increase of thermal conductivity in the axial conduction term while the heat transfer coefficient in the heat exchanger remains unchanged), the temperature profile shape remains almost unchanged until Pe drops to ~10 and below, where a smoother temperature profile emerges because of the strong axial heat conduction effect. Since the system Pe is ~100 000, it is secure to neglect the axial heat conduction term for the prediction of the fluid temperature profile. For the backward circulation case with Pe ~ 1, the temperature profile could not produce the needed buoyancy force, and thus no backward circulation exists. In terms of linear stability analysis, the characteristic frequency has a real positive root without an imaginary component. This is a static instability reflecting the absence of steady-state solutions.

Figure 7 presents the natural circulation solutions in a dimensionless form: a modified Grashof number, defined below, versus the Reynolds number:

$$\mathrm{Gr} = \frac{\rho^2 g \beta \Delta T H_{th}^3}{\mu^2} . \quad (42)$$

The thermal center height H_{th} measures from the heating center to the cooling center, and ΔT is the maximum temperature difference in the closed loop.

The results suggest that the effect of the axial conduction term on the steady-state natural forward and backward circulations is negligible as the Peclet number drops from infinity (without axial heat conduction) to 1000, ~1% of the LBE system. This is because the coolant temperature profile along the natural circulation loop remains almost unchanged within the Peclet number range of this investigation. Namely, neglecting the fluid axial heat conduction term in the steady-state natural circulation analysis is a proper approximation (see Figs. 8 and 9).

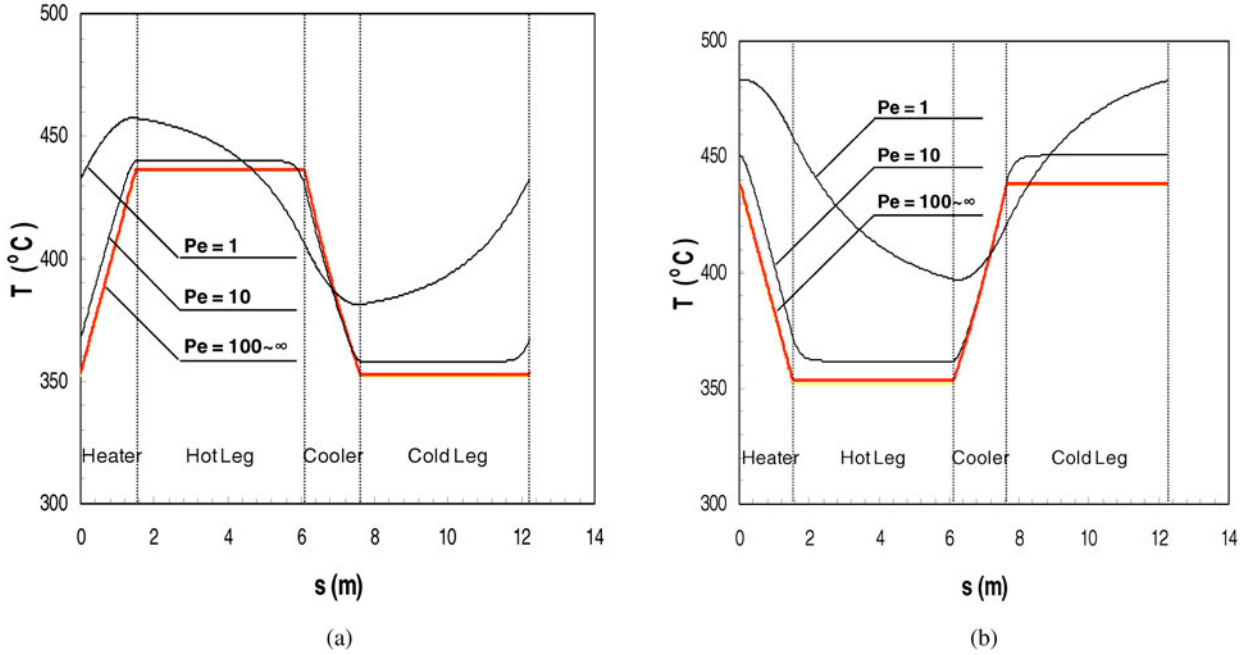

Fig. 6. Steady-state (a) forward and (b) backward circulation temperature profiles.

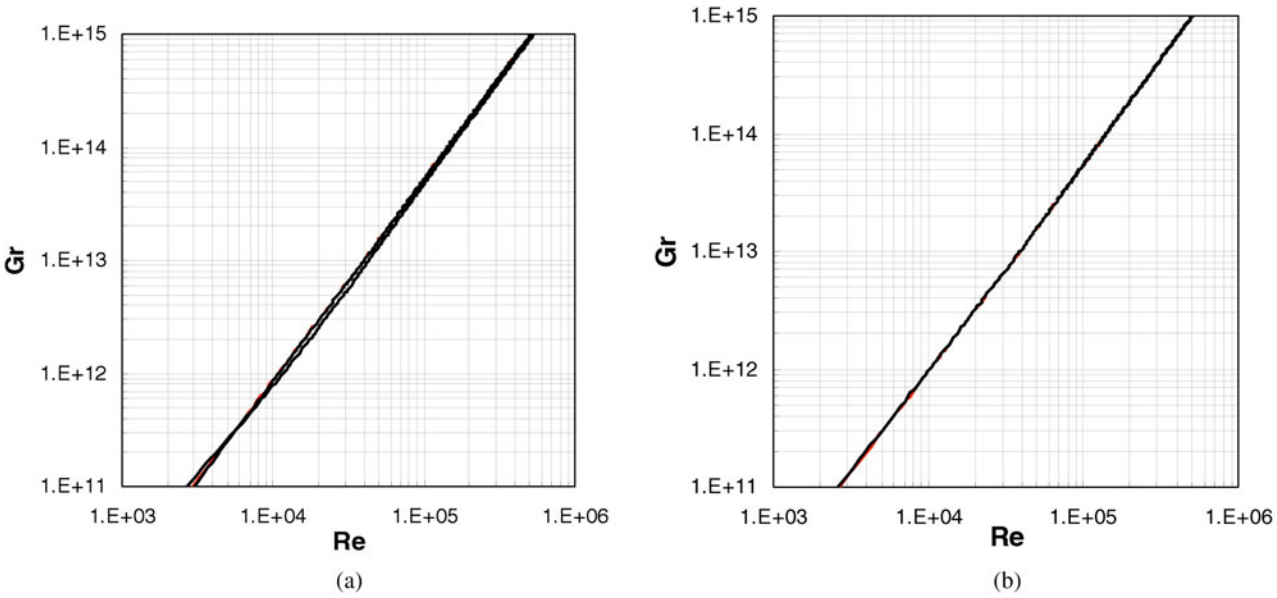

Fig. 7. Steady-state (a) forward and (b) backward circulation solutions (Gr versus Re).

III.C. Linear Perturbation Analysis

For simplicity, the heat transfer coefficient is assumed to be constant in the linear stability analysis. The rationale behind this assumption is that the perturbation is small around the steady solution, and therefore this coefficient is relatively stable.

The major assumption to be made in this simplified analysis is constant flow area in the loop. This assumption is applied to the core heating section, upper plenum, and bottom section. The friction loss due to pipe size difference is lumped into a minor pressure loss coefficient K. All the assumptions are summarized as follows:

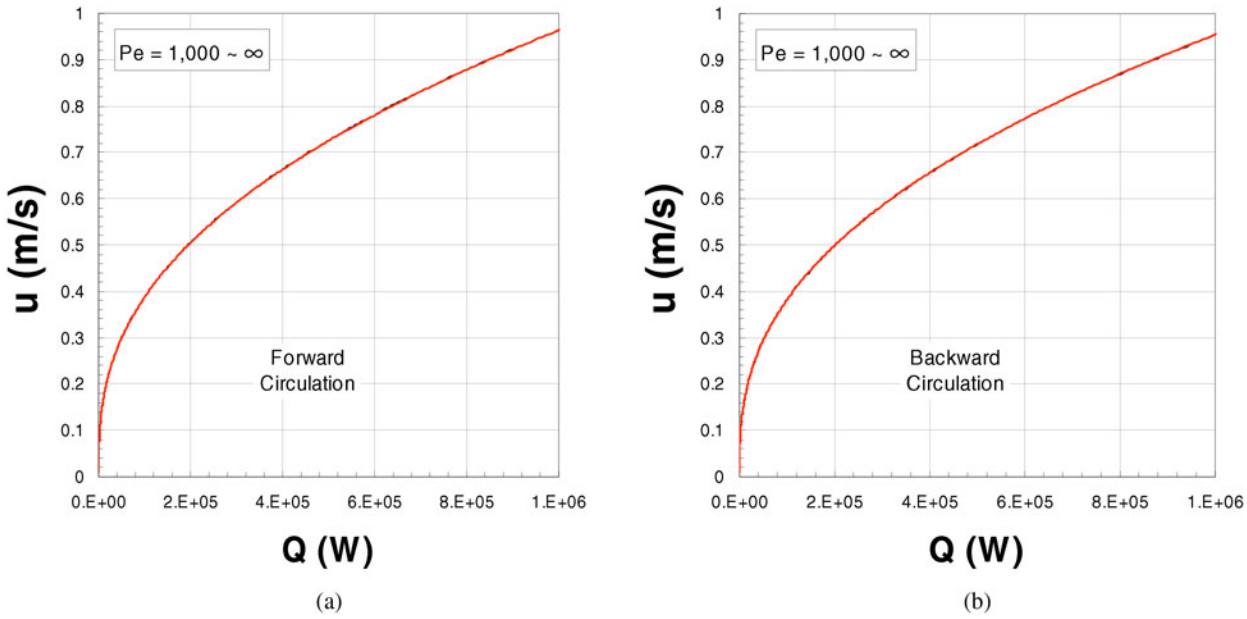

Fig. 8. Core coolant velocity versus power for the steady-state natural (a) forward and (b) backward circulations.

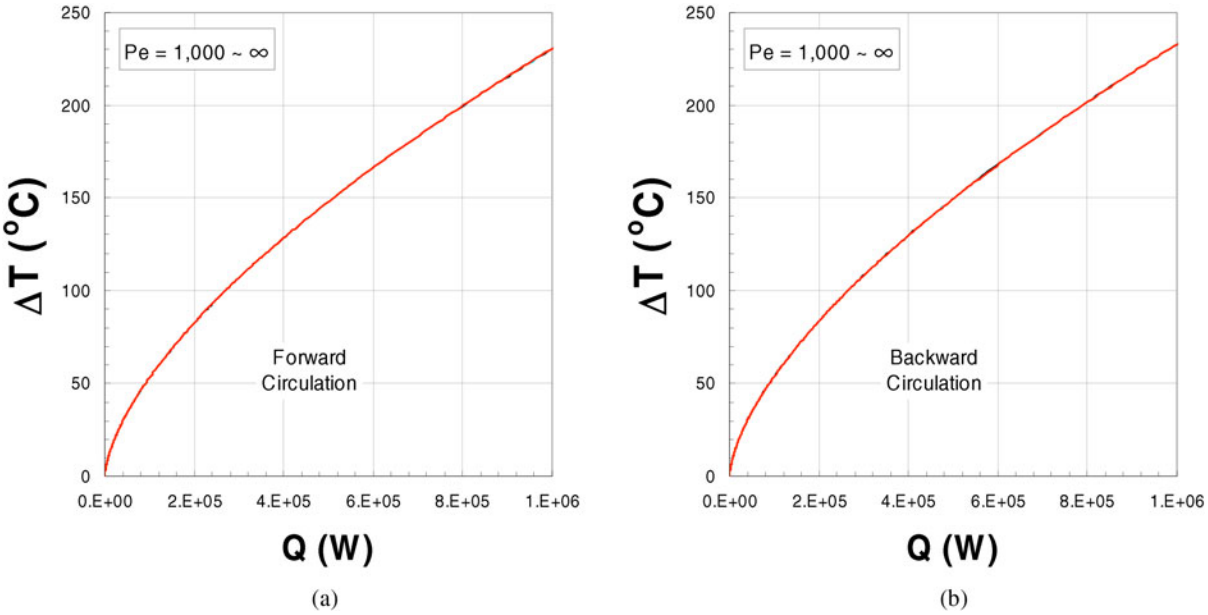

Fig. 9. Temperature increase across the core versus power for the steady-state natural (a) forward and (b) backward circulations.

1. constant flow area
2. no free surface in the upper plenum
3. neglecting the form losses due to two bends in the test loop.

With those assumptions, the simplified test loop is shown schematically in Fig. 10.

Following Welander's approach,[3] small disturbances are superimposed upon the steady-state solutions in the following forms:

$$u = u_s + \varepsilon e^{\omega t} \tag{43}$$

and

$$T = T_s + \eta(s) e^{\omega t} \quad . \tag{44}$$

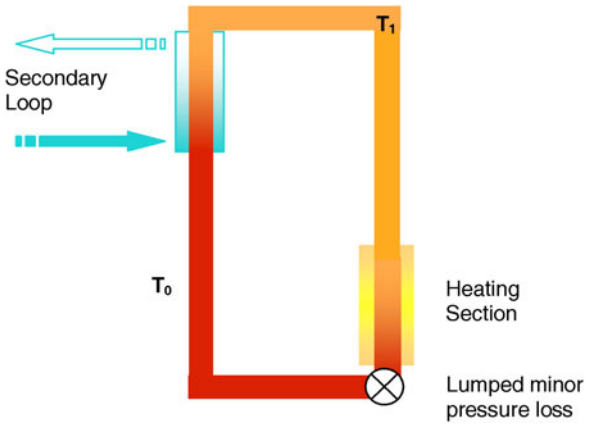

Fig. 10. Simplified loop for the perturbation analysis.

Because of the assumption of constant flow area, the coolant velocity is the same everywhere in the loop. The closed-loop integration of the perturbed momentum equation is given by

$$\rho_0 \varepsilon \omega L = -\rho_0 g \beta \oint \eta \left(\frac{g_s}{g}\right) ds - \rho_0 u_s \varepsilon \left[f\left(\frac{4L}{D}\right)\left(\frac{2-n}{2}\right) + K \right] , \quad (45)$$

where n depends on flow regimes (turbulent flow: $n = 0.25$, $a = 0.317$; laminar flow: $n = 1$, $a = 16$). Assuming a constant heat transfer coefficient, the linearized energy equation is given by

$$\eta\omega + u_s \frac{d\eta}{ds} + \varepsilon \frac{dT_s}{ds} = \begin{cases} \alpha \dfrac{d^2\eta}{ds^2} & \text{Heated region} \\ -\eta h \left(\dfrac{P}{A\rho_0 C}\right) + \alpha \dfrac{d^2\eta}{ds^2} & \text{Heat exchanger region} \\ \alpha \dfrac{d^2\eta}{ds^2} & \text{Others} \end{cases} \quad (46)$$

Equation (46) has to be solved for different flow regions in order to find the closed-loop integration of η, as done previously for steady state. Since the integration depends on the circulation direction, the forward and backward circulations have to be investigated separately.

III.C.1. Forward Circulation

The process is composed of four steps. First, the temperature disturbance distribution in each section has to be solved individually. Second, the closed-loop boundary condition is used to determine the temperature disturbance (at the core inlet) in terms of the steady-state solutions, core coolant velocity disturbance, and characteristic frequency η. Afterward, the closed-loop integration of η ought to be performed, and finally an algebraic equation of ω can be obtained, as done for steady state and further applying the boundary conditions, i.e., continuity in temperature disturbance and its gradient at each pipe junction:

$$\left(\frac{\eta}{\varepsilon}\right)\Big|_{s=L_{CL}}^{CL} = \left(\frac{\eta}{\varepsilon}\right)\Big|_{s=0}^{core} ,$$

$$\left(\frac{\eta}{\varepsilon}\right)\Big|_{s=H_{core}}^{core} = \left(\frac{\eta}{\varepsilon}\right)\Big|_{s=0}^{HL} ,$$

$$\left(\frac{\eta}{\varepsilon}\right)\Big|_{s=L_{HL}}^{HL} = \left(\frac{\eta}{\varepsilon}\right)\Big|_{s=0}^{SG} ,$$

$$\left(\frac{\eta}{\varepsilon}\right)\Big|_{s=H_{SG}}^{SG} = \left(\frac{\eta}{\varepsilon}\right)\Big|_{s=0}^{CL} ,$$

$$\frac{d}{ds}\left(\frac{\eta}{\varepsilon}\right)\Big|_{s=L_{CL}}^{CL} = \frac{d}{ds}\left(\frac{\eta}{\varepsilon}\right)\Big|_{s=0}^{core} ,$$

$$\frac{d}{ds}\left(\frac{\eta}{\varepsilon}\right)\Big|_{s=H_{core}}^{core} = \frac{d}{ds}\left(\frac{\eta}{\varepsilon}\right)\Big|_{s=0}^{HL} ,$$

$$\frac{d}{ds}\left(\frac{\eta}{\varepsilon}\right)\Big|_{s=L_{HL}}^{HL} = \frac{d}{ds}\left(\frac{\eta}{\varepsilon}\right)\Big|_{s=0}^{SG} ,$$

and

$$\frac{d}{ds}\left(\frac{\eta}{\varepsilon}\right)\Big|_{s=H_{SG}}^{SG} = \frac{d}{ds}\left(\frac{\eta}{\varepsilon}\right)\Big|_{s=0}^{CL} .$$

From all the sections using the above-mentioned boundary condition, eight equations are obtained to form a matrix:

$$\begin{bmatrix} -1 & -e^{\lambda_4 H_{core}} & e^{-\lambda_3 L_{HL}} & 1 & 0 & 0 & 0 & 0 \\ -\lambda_3 & -\lambda_4 e^{\lambda_4 H_{core}} & \lambda_3 e^{-\lambda_3 L_{HL}} & \lambda_4 & 0 & 0 & 0 & 0 \\ 0 & 0 & -1 & -e^{\lambda_4 L_{HL}} & e^{-\lambda_5 H_{SG}} & 1 & 0 & 0 \\ 0 & 0 & -\lambda_3 & -\lambda_4 e^{\lambda_4 L_{HL}} & \lambda_5 e^{-\lambda_5 H_{SG}} & \lambda_6 & 0 & 0 \\ 0 & 0 & 0 & 0 & -1 & -e^{\lambda_6 H_{SG}} & e^{-\lambda_3 L_{CL}} & 1 \\ 0 & 0 & 0 & 0 & -\lambda_5 & -\lambda_6 e^{\lambda_6 H_{SG}} & \lambda_3 e^{-\lambda_3 L_{CL}} & \lambda_4 \\ e^{-\lambda_3 H_{core}} & 1 & 0 & 0 & 0 & 0 & -1 & -e^{\lambda_4 L_{CL}} \\ \lambda_3 e^{-\lambda_3 H_{core}} & \lambda_4 & 0 & 0 & 0 & 0 & -\lambda_3 & -\lambda_4 e^{\lambda_4 L_{CL}} \end{bmatrix}$$

$$\times \begin{bmatrix} C''_{11} \\ C''_{12} \\ C''_{13} \\ C''_{14} \\ C''_{15} \\ C''_{16} \\ C''_{17} \\ C''_{18} \end{bmatrix} = \begin{bmatrix} \dfrac{N_1 B_3 e^{-N_1 L_{HL}}}{\omega + Z_1} - \dfrac{N_2}{\omega} - \dfrac{N_1 B_1}{\omega + Z_1} \\ \dfrac{N_1^2 B_3}{\omega + Z_1} e^{-N_1 L_{HL}} - \dfrac{N_1^2 B_1}{\omega + Z_1} \\ \dfrac{B_5 \lambda_1}{\omega + Z_2} + \dfrac{B_6 \lambda_2}{\omega + Z_3} e^{-\lambda_2 H_{SG}} - \dfrac{N_1 B_3}{\omega + Z_1} \\ \dfrac{B_5 \lambda_1^2}{\omega + Z_2} + \dfrac{B_6 \lambda_2^2 e^{-\lambda_2 H_{SG}}}{\omega + Z_3} - \dfrac{N_1^2 B_3}{\omega + Z_1} \\ \dfrac{N_1 B_7}{\omega + Z_1} e^{-N_1 L_{CL}} - \dfrac{B_5 \lambda_1 e^{\lambda_1 H_{SG}}}{\omega + Z_2} - \dfrac{B_6 \lambda_2}{\omega + Z_3} \\ \dfrac{N_1^2 B_7 e^{-N_1 L_{CL}}}{\omega + Z_1} - \dfrac{B_5 \lambda_1^2 e^{\lambda_1 H_{SG}}}{\omega + Z_2} - \dfrac{B_6 \lambda_2^2}{\omega + Z_3} \\ \dfrac{N_2}{\omega} + \dfrac{N_1 B_1}{\omega + Z_1} e^{-N_1 H_{core}} - \dfrac{N_1 B_7}{\omega + Z_1} \\ \dfrac{N_1^2 B_1 e^{-N_1 H_{core}}}{\omega + Z_1} - \dfrac{N_1^2 B_7}{\omega + Z_1} \end{bmatrix} ,$$

where

$$N_1 \Lambda_1 = \lambda_1 \ , \tag{47}$$

$$N_1 \Lambda_2 = \lambda_2 \ , \tag{48}$$

$$Z = \frac{hP_{SG}}{A_{SG} \rho_0 C} \ , \tag{49}$$

$$Z_1 = -\alpha N_1^2 + u_s N_1 \ , \tag{50}$$

$$Z_2 = -\alpha (\lambda_1)^2 + u_s \lambda_1 + Z \ , \tag{51}$$

$$Z_3 = -\alpha (\lambda_2)^2 + u_s \lambda_2 + Z \ , \tag{52}$$

$$\alpha = \frac{\kappa}{\rho c} \ ,$$

$$\lambda_1 = N_1 \times \Lambda_1 \ ,$$

$$\lambda_2 = N_1 \times \Lambda_2 \ ,$$

$$\lambda_3 = \frac{u_s + \sqrt{u_s^2 + 4\alpha\omega}}{2\alpha} \ ,$$

$$\lambda_4 = \frac{u_s - \sqrt{u_s^2 + 4\alpha\omega}}{2\alpha} \ ,$$

$$\lambda_5 = \frac{u_s + \sqrt{u_s^2 + 4\alpha\left(\omega + \dfrac{hP}{A\rho c}\right)}}{2\alpha} \ ,$$

and

$$\lambda_6 = \frac{u_s - \sqrt{u_s^2 + 4\alpha\left(\omega + \frac{hP}{A\rho c}\right)}}{2\alpha} \ .$$

The solution of this linear algebraic equation set provides a relation between the temperature disturbance and the velocity disturbance. To obtain the final solution of the characteristic frequency, the temperature disturbance integration over the entire loop needs to be carried out in the perturbed integral momentum equation.

Now for the buoyancy term we have

$$M_1 = \oint -\rho\beta\left(\frac{g_s}{g}\right)\eta e^{\omega t}\, ds \ , \tag{53}$$

$$M_1 = \rho\beta g\left[\int_0^{H_{core}}\left(\frac{\eta}{\varepsilon}\right)_{core} ds + \int_0^{H_{HL}}\left(\frac{\eta}{\varepsilon}\right)_{HL} ds - \int_0^{H_{SG}}\left(\frac{\eta}{\varepsilon}\right)_{SG} ds - \int_0^{H_{CL}}\left(\frac{\eta}{\varepsilon}\right)_{CL} ds\right] , \tag{54}$$

$$\begin{aligned} M_1 = \rho\beta g\Bigg[& \frac{C_{11}''}{\lambda_3} + \frac{C_{12}'' e^{\lambda_4 H_{core}}}{\lambda_4} - \frac{N_2 H_{core}}{\omega} - \frac{B_1}{\omega + Z_1} - \frac{C_{11}'' e^{-\lambda_3 H_{core}}}{\lambda_3} - \frac{C_{12}''}{\lambda_4} + \frac{B_1}{\omega + Z_1} e^{-N_1 H_{core}} + \frac{C_{13}'' e^{-\lambda_3 (L_{HL} - H_{HL})}}{\lambda_3} \\ & + \frac{C_{14}'' e^{\lambda_4 H_{HL}}}{\lambda_4} - \frac{B_3}{Z_1 + \omega} e^{-N_1 (L_{HL} - H_{HL})} - \frac{C_{13}'' e^{-\lambda_3 L_{HL}}}{\lambda_3} - \frac{C_{14}''}{\lambda_4} + \frac{B_3}{Z_1 + \omega} e^{-N_1 L_{HL}} - \frac{C_{15}''}{\lambda_5} - \frac{C_{16}'' e^{\lambda_6 H_{SG}}}{\lambda_6} \\ & + \frac{B_5 e^{\lambda_1 s}}{Z_2 + \omega} + \frac{B_6}{Z_3 + \omega} + \frac{C_{15}'' e^{-\lambda_5 H_{SG}}}{\lambda_5} + \frac{C_{16}''}{\lambda_6} - \frac{B_5}{Z_2 + \omega} - \frac{B_6 e^{-\lambda_2 H_{SG}}}{Z_3 + \omega} - \frac{C_{17}'' e^{-\lambda_3 (L_{CL} - H_{CL})}}{\lambda_3} - \frac{C_{18}'' e^{\lambda_4 H_{CL}}}{\lambda_4} \\ & + \frac{B_7}{Z_1 + \omega} e^{-N_1 (L_{CL} - H_{CL})} + \frac{C_{17}'' e^{-\lambda_3 L_{CL}}}{\lambda_3} + \frac{C_{18}''}{\lambda_4} - \frac{B_7}{Z_1 + \omega} e^{-N_1 L_{CL}}\Bigg] . \end{aligned} \tag{55}$$

III.C.2. Backward Circulation

The matrix is the same as obtained previously in forward circulation. The only difference lies in the buoyancy term:

$$M_1 = \rho\beta g\left[-\int_0^{H_{core}}\left(\frac{\eta}{\varepsilon}\right)_{core} ds + \int_{L_{CL} - H_{CL}}^{L_{CL}}\left(\frac{\eta}{\varepsilon}\right)_{HL} ds + \int_0^{H_{SG}}\left(\frac{\eta}{\varepsilon}\right)_{SG} ds - \int_{L_{HL} - H_{HL}}^{L_{HL}}\left(\frac{\eta}{\varepsilon}\right)_{CL} ds\right] , \tag{56}$$

$$\begin{aligned} M_1 = \rho\beta g\Bigg[& -\frac{C_{11}''}{\lambda_3} - \frac{C_{12}'' e^{\lambda_4 H_{core}}}{\lambda_4} + \frac{N_2 H_{core}}{\omega} + \frac{B_1}{\omega + Z_1} + \frac{C_{11}'' e^{-\lambda_3 H_{core}}}{\lambda_3} + \frac{C_{12}''}{\lambda_4} - \frac{B_1}{\omega + Z_1} e^{-N_1 H_{core}} \\ & + \frac{C_{13}'' e^{-\lambda_3 (L_{HL} - L_{CL})}}{\lambda_3} + \frac{C_{14}'' e^{\lambda_4 L_{CL}}}{\lambda_4} - \frac{B_3}{\omega + Z_1} e^{-N_1 (L_{HL} - L_{CL})} - \frac{C_{13}'' e^{-\lambda_3 (L_{HL} - L_{CL} + H_{CL})}}{\lambda_3} - \frac{C_{14}'' e^{\lambda_4 (L_{CL} - H_{CL})}}{\lambda_4} \\ & + \frac{B_3}{\omega + Z_1} e^{-N_1 (L_{HL} - L_{CL} + H_{CL})} + \frac{C_{15}''}{\lambda_5} + \frac{C_{16}'' e^{\lambda_6 H_{SG}}}{\lambda_6} - \frac{B_5 e^{\lambda_1 H_{SG}}}{Z_2 + \omega} - \frac{B_6}{Z_3 + \omega} - \frac{C_{15}'' e^{-\lambda_5 H_{SG}}}{\lambda_5} - \frac{C_{16}''}{\lambda_6} \\ & + \frac{B_5}{Z_2 + \omega} + \frac{B_6 e^{-\lambda_2 H_{SG}}}{Z_3 + \omega} - \frac{C_{17}'' e^{-\lambda_3 (L_{CL} - L_{HL})}}{\lambda_3} - \frac{C_{18}'' e^{-\lambda_4 L_{HL}}}{\lambda_4} - \frac{B_7}{Z_1 + \omega} e^{-N_1 (L_{CL} - L_{HL})} \\ & + \frac{C_{17}'' e^{-\lambda_3 (L_{CL} - L_{HL} + H_{HL})}}{\lambda_3} + \frac{C_{18}'' e^{\lambda_4 (L_{HL} - H_{HL})}}{\lambda_4} - \frac{B_7}{Z_1 + \omega} e^{-N_1 (L_{CL} - L_{HL} + H_{HL})}\Bigg] . \end{aligned} \tag{57}$$

For both cases, i.e., forward and backward circulations, we have

$$F(\omega) = M_1 - FF - L\rho_0\omega = 0 \ , \tag{58}$$

where

$$FF = \rho u f \left(\frac{4L}{D}\right)\left(\frac{2-n}{2}\right) \tag{59}$$

and the value of M_1 is obtained from Eq. (55) for forward circulation and from Eq. (57) for backward circulation. M_1 represents the buoyancy term for the circulation loop and FF represents the friction term, and the value for f can be obtained by referring to Eqs. (37), (38), and (39). $F(\omega)$ is further evaluated in MATLAB, and stability is determined using the Nyquist criterion and a numerical root-search method. With the solution of temperature perturbation as a function of velocity disturbance, the perturbed linear momentum equation can yield an algebraic characteristic equation that governs the angular frequency ω. If the root of ω has a positive real component, the system is unstable because a small disturbance will grow exponentially. Otherwise, the system should be stable or neutrally stable.

IV. STABILITY BOUNDARY

Two mathematical approaches were employed to assess the system stability: the Nyquist criterion and a root-searching method.[15] With the Nyquist criterion, the stability boundary can be readily identified without the complication of searching for each individual root. Since the Nyquist criterion cannot provide the actual value of the root, it is difficult to address the mechanisms that govern the system's stability. Therefore, the root-search method is employed to search for the root as a function of the Reynolds number.

IV.A. The Nyquist Criterion

The Nyquist criterion basically provides a method to investigate whether Eq. (58) has roots in the ω plane with a positive real component. According to the criterion, the number of roots of Eq. (58) within a given closed curve in the ω plane is equal to the number of times $F(\omega)$ encircles the origin in the F plane as ω traverses the given closed curve. $F(\omega)$ must be analytic within, and analytic and nonzero on, the closed curve. In Fig. 11, the positive imaginary branch of the closed curve in the ω plane is shown by the solid curve in the $F(\omega)$ plane, whereas the negative branch corresponds to the dotted line. Figure 11a shows that the curve in the $F(\omega)$ plane does not enclose the origin, and therefore the system is stable for forward circulation, whereas Fig. 11b shows that the curve in the $F(\omega)$ plane does enclose the origin, and therefore the system is unstable for backward circulation.

IV.B. Root-Search Method

In the root-search method, effort focuses on the lowest characteristic frequency and on the root that may have a positive real component. Figure 12 presents two plots of $|F(\omega)|$ versus ω for both forward and backward circulation. In this study the main objective is to find the minimum magnitude of function $F(\omega)$ by varying ω. For the forward circulation, with nominal power (0.206 MW) minimum $|F(\omega)|$ lands at a point where the real part of ω is negative; this implies a stable condition if $|F(\omega)|$ truly touches zero at that location. On the other hand, for backward circulation, with nominal power (0.206 MW) minimum $|F(\omega)|$ lands at a point where the real part of ω is positive; this implies an unstable condition.

Using MATLAB solver code, a root-searching program was developed to follow one specific root as the

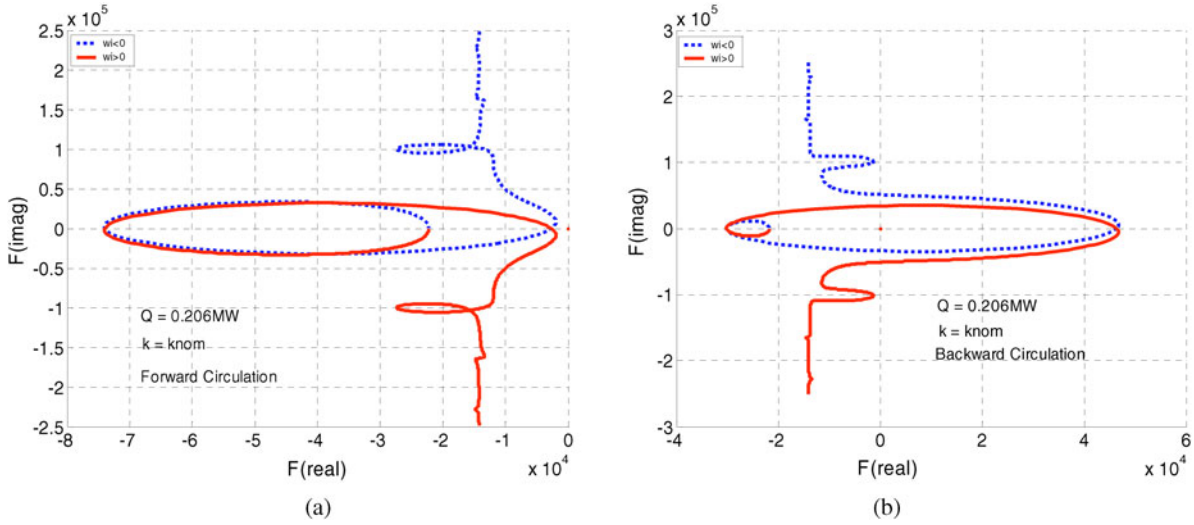

Fig. 11. Nyquist plot of $F(\omega)$ for (a) forward and (b) backward circulation.

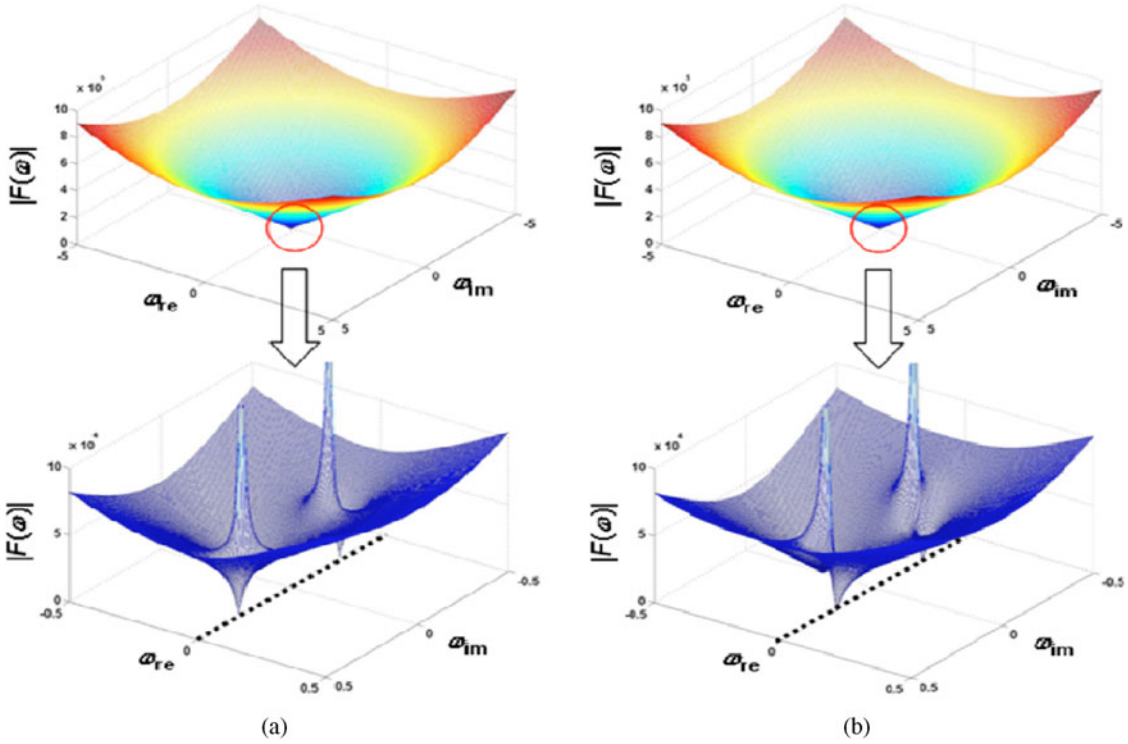

Fig. 12. Three-dimensional surface plots of $F(\omega)$ for (a) forward and (b) backward circulation.

heating power increases. Figure 13 summarizes the results for both forward and backward circulations. The real component of the root against the Reynolds number is shown in Fig. 13a for the Peclet number ranging from 1000 to infinity. For forward circulation, there is an unstable region where $\omega_{re} > 0$. Interestingly, as the Peclet number decreases, the unstable region becomes smaller and the circulation is thus more stable. This is possibly due to the smoother temperature profile, which has a damping effect on disturbances. However, the variation is very small within the Peclet number range. On the other hand, the backward circulation becomes unstable at a relatively low Reynolds number ($\sim 8 \times 10^3$). This characteristic is preferable for reactor operation. When external heating is applied to melt liquid metal, a backward circulation could be established initially. Once the core heats up, the backward circulation might quickly turn around due to the flow instability. Nevertheless, the results in Fig. 13a suggest that fluid axial heat conduction has no effect on the stability boundary within the wide Peclet number range. The imaginary component of ω versus Reynolds number is plotted in Fig. 13b. The Peclet number in the specified range seems to have no effect on ω_{im} for both backward and forward circulation. The value of ω_{im} matches roughly the frequency of a fluid particle passing through the entire circulation loop, in spite of the power level change that results in the variation of the fluid circulating velocity. This result may imply that a disturbance could be enhanced after traveling around the loop when instability occurs. More important, if the frequency matches a certain neutronics feedback period, resonance oscillations could emerge, resulting in linearly unstable natural circulations.

V. CONCLUSIONS

1. A relatively complete analysis method is developed to solve one-dimensional natural circulation problems with the consideration of fluid axial heat conduction effect through nondimensional analysis, steady-state solution estimation, and linear perturbation analysis.

2. Under steady-state conditions, the energy equation is integrated into each pipe section (i.e., heated, hot, heat exchanger, cold). Temperature/flux continuity is imposed as the boundary condition at each pipe junction; thus, eight equations are obtained and further solved to obtain temperature distribution. By substituting the closed-loop temperature integration into the integral momentum equation, an algebraic equation of fluid velocity is obtained.

3. From steady-state analysis depending on flow direction, two separate cases are investigated (i.e., forward circulation and backward circulation). At nominal power (0.206 MW), 0.5014 m/s velocity was obtained for

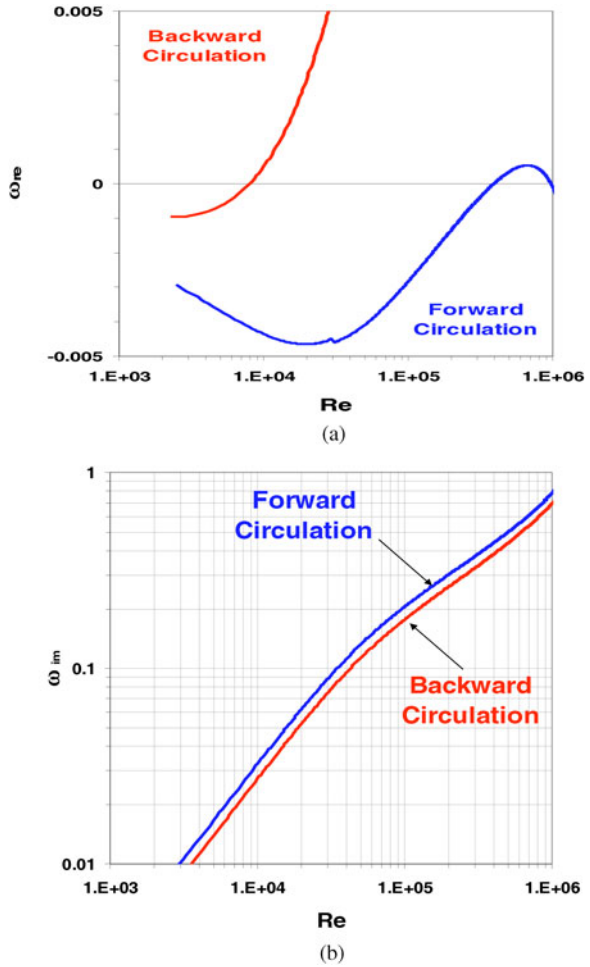

Fig. 13. (a) Real and (b) imaginary components of ω versus Reynolds number.

forward circulation and 0.4956 m/s velocity for backward circulation. To more fully understand the fluid axial conduction term effect, the power was varied from 0.24 W to 6.48 MW. A common trend was discovered for both (i.e., as the Reynolds number is increased, the system tends to approach an unstable state).

4. Thermal conductivity is artificially increased in the axial conduction term. The temperature profile remains almost unchanged until the Peclet number drops to ~10 and below. When the Peclet number is ~1, no backward circulation exists since the temperature profile is not able to produce the needed buoyancy force.

5. The steady-state solution is perturbed and the energy equation is integrated in each pipe section. Temperature and flux continuity is imposed at the boundary condition at each pipe junction. The closed-loop boundary condition is used to determine the temperature disturbance in terms of the steady-state solutions, core coolant velocity disturbance, and characteristic frequency ω. To obtain the final solution of characteristic frequency, the temperature disturbance integration over the entire loop is carried out in the perturbed integral momentum equation. Two mathematical approaches were employed to assess the system stability: the Nyquist criterion and a root-searching method. A stable system was found for forward circulation, whereas under the same nominal power condition, backward circulation was found to be unstable. Both the Nyquist criterion and the root-search method produced consistent results for the linear stability analysis.

6. Fluid axial heat conduction in the natural circulation loop should be considered only when the modified Peclet number is ~1 or below, which is significantly smaller than the practical value (100 000 in the specified loop) of liquid metal natural circulation systems. Therefore, it is appropriate to neglect the fluid axial heat conduction effect in the thermal-hydraulic analysis related to liquid metal natural circulation–cooled nuclear reactors. However, at low heating power conditions, as in the case of reactor start-up or long-term cooling after shutdown, fluid axial thermal conduction could become important because of the slow coolant natural circulation. In those cases, the magnitude of the system Peclet number should be closely examined to validate the neglecting of fluid axial heat conduction in natural circulation analysis.

VI. DISCUSSION AND FUTURE WORK

1. Stable backward circulation is possible if the Reynolds number and the loop friction loss are small. Experimentally, such flow may be initiated with an external driving force or heating. It is speculated that for large disturbances, the flow may be unstable due to nonlinear effects, the resulting flow reversal that leads to a stable forward circulation.

2. Forward flow can be unstable if the Reynolds number exceeds a critical limit for the case of no minor pressure loss. Physically, flow reversal due to flow oscillation is unlikely for the specific loop geometry and the unstable nature of the backward circulation. Eventually, the disturbance should calm down, perhaps because of the nonlinear effects and/or the axial heat conduction.

With the knowledge and experience gained, we would like to propose future efforts for the improvement and modification of the study:

1. Carry out the same analysis with consideration of area change and free surface in the upper plenum.

2. Conduct a parametric study on the loop geometry. By varying the locations and sizes of the heated region and heat exchanger, certain design criteria are expected from the analysis, which could be very useful for the development of inherently safe Generation IV reactors.

3. Use numerical simulations to investigate the nonlinear effects on flow stability, particularly on the evaluation of the linear stability boundary. The results could also provide guidance to the experimental investigations on the transient behaviors of the model reactor.

NOMENCLATURE

A = flow area (m^2)

A_{SG} = flow area of the heat exchanger (primary) (m^2)

a = constant used in the friction factor correlation

B_1 through B_8 = integration constants for steady-state fluid temperature in different regions

C = fluid specific heat ($J/kg \cdot °C^{-1}$)

C_1 through C_8 = integration constants for homogeneous solutions of steady-state fluid temperature in different regions

C''_{11} through C''_{18} = integration constants for the ratios of the fluid temperature perturbation to velocity perturbation in different regions

D_h = hydraulic equivalent diameter (m)

f = friction factor

g = gravitational constant (m/s^2)

g_s = flow directional component of the gravitational acceleration vector (m/s^2)

H_{CL} = height of the cold leg (m)

H_{core} = flow path height of the reactor core (m)

H_{HL} = height of the hot leg (m)

H_{SG} = flow path height of the heat exchanger (primary) (m)

h = heat transfer coefficient ($J/m^2 \cdot s^{-1}$ per °C)

K = form pressure loss coefficient

k = fluid thermal conductivity ($J/m^2 \cdot s^{-1}$ per °C)

k_{nom} = nominal value of fluid thermal conductivity ($J/m^2 \cdot s^{-1}$ per °C)

L_{CL} = flow path length of the cold leg (m)

L_{HL} = flow path length of the hot leg (m)

L_{loop} = total flow path length of the natural circulation loop (m)

n = constant used in the friction factor correlation

P = wetted perimeter (m)

P_h = heated perimeter (m)

p = pressure (N/m^2)

q''_w = wall heat flux ($J/m^2 \cdot s^{-1}$)

Re = Reynolds number, $\rho u D_h/\mu$

s = flow directional coordinate (m)

T = fluid temperature (°C)

T_{CL} = steady-state fluid temperature in the cold leg (°C)

T_{core} = steady-state fluid temperature in the reactor core (°C)

T_{HL} = steady-state fluid temperature in the hot leg (°C)

T_{ref} = reference fluid temperature (°C)

T_s = steady-state fluid temperature (°C)

T_{SG} = steady-state fluid temperature in the heat exchanger (primary) (°C)

T_w = wall temperature (°C)

t = time (s)

u = one-dimensional fluid velocity (m/s)

u_s = steady-state one-dimensional fluid velocity (m/s)

$\in$ = relative error for convergence of numerical iterations

Greek

α = fluid thermal diffusivity (m^2/s)

β = fluid volumetric thermal expansion coefficient (1/°C)

ε = initial magnitude of the fluid velocity perturbation (m/s)

η = initial magnitude of the fluid temperature perturbation (°C)

η_{CL} = initial magnitude of the fluid temperature perturbation in the cold leg (°C)

η_{core} = initial magnitude of the fluid temperature perturbation in the reactor core (°C)

η_{HL} = initial magnitude of the fluid temperature perturbation in the hot leg (°C)

η_{SG} = initial magnitude of the fluid temperature perturbation in the heat exchanger (°C)

$\lambda_{1,2}$ = roots of the characteristic equation corresponding to a homogeneous differential equation for the steady-state fluid temperature in the heat exchanger (m^{-1})

$\lambda_{3,4}$ = roots of the characteristic equation corresponding to a homogeneous differential equation for the fluid temperature perturbation in the reactor core (m^{-1})

$\lambda_{5,6}$ = roots of the characteristic equation corresponding to a homogeneous differential equation for the fluid temperature perturbation in the heat exchanger (m^{-1})

μ = fluid dynamic viscosity ($kg/m \cdot s$)

ρ = fluid density (kg/m^3)

ρ_0 = fluid density at a reference fluid temperature (kg/m^3)

τ_w = wall shear stress (N/m^{-2})

ω = characteristic angular frequency (s^{-1})

Subscripts

CL = cold leg

core = reactor core

H = homogeneous solution

HL = hot leg

i, j = region index

loop = natural circulation loop

loss = heat loss

P = perturbation; particular solution

SG = heat exchanger

s = flow directional component

w = wall

Dimensions

[*L*] = length

[*M*] = mass

[*T*] = time

[—] = dimensionless

ACKNOWLEDGMENTS

This work was supported by Argonne National Laboratory under the U.S. NERI program.

REFERENCES

1. E. P. LOEWEN and A. T. TOKUHIRO, "Status of Research and Development of the Lead-Alloy-Cooled Fast Reactor," *J. Nucl. Sci. Technol.*, **40**, *8*, 614 (2003).

2. J. B. KELLER, "Periodic Oscillations in a Model of Thermal Convection," *J. Fluid Mech.*, **26**, *3*, 599 (1966).

3. P. WELANDER, "On the Oscillatory Instability of a Differentially Heated Fluid Loop," *J. Fluid Mech.*, **29**, 17 (1967).

4. H. F. CREVELING, J. F. DE PAZ, J. Y. BALADI, and R. J. SCHOENHALS, "Stability Characteristics of a Single-Phase Free Convection Loop," *J. Fluid Mech.*, **67**, 65 (1975).

5. P. K. VIJAYAN, H. AUSTREGESILO, and V. TESCHENDORFF, "Simulation of the Unstable Oscillatory Behavior of Single-Phase Natural Circulation with Repetitive Flow Reversals in a Rectangular Loop Using the Computer Code ATHLET," *Nucl. Eng. Des.*, **155**, 623 (1995).

6. H. H. BAU and K. E. TORRANCE, "On the Stability and Flow Reversal of an Asymmetrically Heated Open Convection Loop," *J. Fluid Mech.*, **109**, 417 (1981).

7. Y. ZVIRIN, P. R. JEUCK, C. R. SULLIVAN, and R. B. DUFFY, "Experimental and Analytical Investigation of a Natural Circulation System with Parallel Loops," *J. Heat Transfer*, **103**, 645 (1981).

8. Y. ZVIRIN, "A Review of Natural Circulation Loops in Pressurized Water Reactors and Other Systems," *Nucl. Eng. Des.*, **67**, 203 (1981).

9. E. V. DEPIANTE, "Stability Analysis of a Linear Reactor System with Feedback Under Low-Flow, Low-Power Conditions," *Nucl. Sci. Eng.*, **113**, 251 (1993).

10. Q. WU and J. J. SIENICKI, "Stability Analysis on Single-Phase Natural Circulation in Argonne Lead Loop Facility," *Nucl. Eng. Des.*, **224**, *1*, 23 (2003).

11. B. W. SPENCER et al., "An Advanced Modular HLMC Reactor Concept Featuring Economy, Safety, and Proliferation Resistance," *Proc. Eighth Int. Conf. Nuclear Engineering* (ICONE-8), Baltimore, Maryland, April 2–6, 2000.

12. J. J. SIENICKI and B.W. SPENCER, "Power Optimization in the STAR-LM Generation IV Modular, Natural Convection Reactor System," *Proc. Tenth Int. Conf. Nuclear Engineering* (ICONE 10), paper 10-22294, Arlington, Virginia, April 14–18, 2002.

13. P. N. MARTYNOV and K. D. IVANOV, "Properties of Lead-Bismuth Coolant and Perspectives of Non-Electric Applications of Lead-Bismuth Reactor," XA9848814, TECDOC 1056, pp. 177–184 Institute for Physics and Power Engineering, Russian Federation (1998).

14. H. NINOKATA, A. P. SOROKIN, and P. L. KIRILLOV, "Comparison of Sodium and Lead/Lead-Bismuth as a Coolant and LMFR Safety," *Proc. Eighth Int. Conf. Nuclear Engineering* (ICONE-8), Baltimore, Maryland, April 2–6, 2000.

15. Y. J. YOO, P. SABHARWALL, J. N. REYES, Q. WU, and J. J. SIENICKI, "Effects of Fluid Axial Conduction on Liquid Metal Natural Circulation and Linear Stability," *Proc. Annual Conf. American Nuclear Society*, pp. 1523–1530 (2003).